geosciences

MDPI

Article

Insights on the Formation Conditions of Manganese Oxides from Crimora, VA (USA)

Chiara Elmi [1,*], Jacob R. Whitlock [1], Matthew T. Macdowell [2] and Richard D. Foust, Jr. [2]

[1] Department of Geology and Environmental Science, James Madison University, Harrisonburg, VA 22807, USA
[2] Department of Chemistry and Biochemistry, James Madison University, Harrisonburg, VA 22807, USA; foustrd@jmu.edu (R.D.F.J.)
* Correspondence: elmicx@jmu.edu

Abstract: Many regions of the United States contain manganese deposits economically valuable in New England, Appalachian, and Piedmont regions in the Eastern United States, in Northern Arkansas, and, to a small extent, in Central–Western California. Mn oxide/hydroxide (commonly referred to as Mn oxide minerals) are found in a wide variety of geological settings and occur as fine-grained aggregates, veins, marine and freshwater nodules and concretions, crusts, dendrites, and coatings on rock surfaces (e.g., desert varnish). How manganese oxides form and what mechanisms determine which oxides are likely to form are limited and still debated. This paper focuses on Mn oxides collected at the southern bound of the abandoned open-pit site called Crimora Mine (Augusta County, Virginia). This study uses mineralogical and chemical features to shed light on the origin of manganese deposits in Crimora along the western foot of the Blue Ridge in South–West Virginia. We report the first detailed study on the genesis of the Crimora manganese deposit conducted since the mine was closed in the 1950s. Crimora Mine sample is dark black fine- to medium-grained round and oblong nodules coated with a fine-grained intermix of yellowish earthy limonite, clays, and quartz. Scanning electron microscopy (SEM) revealed that the Crimora Mn-oxides exhibit concentric layering, breccia-like matrices, and veins. X-ray powder diffraction (XRPD) identified the set of Mn minerals as hollandite and birnessite. The concentration and range of dissolved chemical species in freshwater, seawater, and hydrothermal depositional fluids impart a geochemical signature to the Mn-oxides, providing a diagnostic tool to shed light on their genetic origin. Inductively coupled plasma optical emission spectroscopy (ICP-OES) analysis of the Crimora manganese oxides shows Mn, Fe, and Ti, as well as trace elements such as Co, Ba, Y, Zn, Cr, Ni, Tl, La, V, and Li. A bivariate analysis based on the geochemical correlation of Mn and other common substituting cations (e.g., Fe, Co, Ti) shows a mixed genesis in different environments with varying biological and sedimentary supergene (freshwater and marine) conditions. These data suggest that the Mn-rich deposit in Crimora, VA, was formed in a continental margin environment of surficial deposits and reprecipitated in mixed biogenic and supergene conditions.

Keywords: Mn-oxides; genesis; Crimora mine (VA); XRPD; SEM; ICP-OES

check for updates

Citation: Elmi, C.; Whitlock, J.R.; Macdowell, M.T.; Foust, R.D., Jr. Insights on the Formation Conditions of Manganese Oxides from Crimora, VA (USA). *Geosciences* **2023**, *13*, 235. https://doi.org/10.3390/geosciences13080235

Academic Editors: Angelos G. Maravelis and Jesus Martinez-Frias

Received: 19 June 2023
Revised: 31 July 2023
Accepted: 5 August 2023
Published: 8 August 2023

Copyright: © 2023 by the authors. Licensee MDPI, Basel, Switzerland. This article is an open access article distributed under the terms and conditions of the Creative Commons Attribution (CC BY) license (https://creativecommons.org/licenses/by/4.0/).

1. Introduction

Manganese (Mn) is the tenth most abundant element in the Earth's lithosphere. Mn has three different oxidation states with varying properties, Mn^{2+}, Mn^{3+}, and Mn^{4+}. The Mn-O molecule commonly has a six-fold coordination. Mn can form over thirty oxides because of its different oxidation states and octahedral coordination [1]. The structural diversity of manganese oxides results in a different crystallization pathway in solution due to subtle variations in pH and redox potential. The changes in solution chemistry can lead to a non-equilibrium crystallization pathway through different metastable intermediates [2]. Complex natural manganese oxides have been the most abundant nanophases found on Earth since before the Great Oxidation Event, and the Mn cycle is one of the most

important biogeochemical processes on the Earth's surface [3]. Natural manganese oxides are commonly found as a coating on host rocks but can form crystalline structures in several environments, from oceanic hydrothermal deposits to terrestrial manganese deposits formed by hydrothermal, sedimentary, and continental weathering processes [3–7].

Manganese deposits show a variable chemical composition due to the deposition conditions of both ore and host rocks [4,7]. The variable Mn concentration and deposit distributions are controlled by the oxygen flow rate, oxidation potential (Eh) of manganese-bearing solutions, the residence time of Mn in solution, the acidity (pH), and temperature of the solution [8,9]. Generally, manganese solubility (most soluble is Mn^{2+}) is highest at lower pH and lower Eh conditions. The variability in manganese chemical behavior under different physical-chemical conditions results in a possible genesis of Mn deposits from a mixed hydrothermal, biogenic, or diagenetic source [1,10]. The most common manganese deposits form in sedimentary and submarine conditions. Several manganese deposits result from the deposition of Mn-rich sediments on oceans seabed [1,11–15]. Secondary enrichment in marine sedimentary rocks by continental weathering can form high-grade manganese ore deposits (supergene ores) [16–19]. The most common manganese ore minerals include pyrolusite (MnO_2), which is found as grey to black coating and radiating fibrous aggregates in sedimentary and hydrothermally altered rocks, as well as in secondary accumulations [9].

Many regions of the United States contain manganese deposits, but economically valuable ones are uncommon. They have been extensively mined in New England, Appalachian, and Piedmont regions in the Eastern United States, in Northern Arkansas, and, to a smaller extent, in Central–Western California [20]. Deposits of manganese and iron oxides are abundant in the Shenandoah Valley, Virginia (USA) and have been mined for more than 100 years [21]. Virginia supplied the increasing demand for manganese oxides for the steel industry from 1880 to 1914 [22].

Despite manganese oxides' economic and environmental significance, geoscientists continue to debate how manganese oxides form and what mechanisms determine which oxides are likely to form. The origin of manganese oxide deposits in the Shenandoah Valley is unsettled, and the clear mineralogical identification of the manganese oxides and geochemical features are limited. This paper focuses on Mn oxides collected at the southern bound of the abandoned open-pit site called Crimora Mine (Augusta County, Virginia). This study uses mineralogical and chemical features to shed light on the origin of manganese deposits in Crimora that occur along the western foot of the Blue Ridge Mountains.

2. Materials and Methods

2.1. Sampling Location

The manganese ore deposit in this study is located 4 km from the town of Crimora, Augusta County, VA (USA). It was the largest manganese mine in the United States of America: over 160,000 tons of manganese were mined in the period of maximum production from 1882 to 1915 [22–24]. The mine area is scattered along an area of about 0.8 km^2 [21] and runs N–S with a depth of about 1 m and a length of about 280 m [25]. After discovering a substantial concentration of manganese in 1867, open-pit Crimora mines were bought and sold several times, eventually closing operations in 1958 [24].

Today, a hilltop landscape created by mining excavation is a field overlooking the Blue Ridge Mountains. The former mine property has been split between a private residency at the North end and a lake resort at the southern end. Selected sampling sites were at the southern end of the Crimora ore deposit (Figure 1). Samples are dark-black fine-to-medium-grained round and oblong nodules coated with a very fine-grained intermix of yellowish earthy limonite, clays, and quartz (Figure 2).

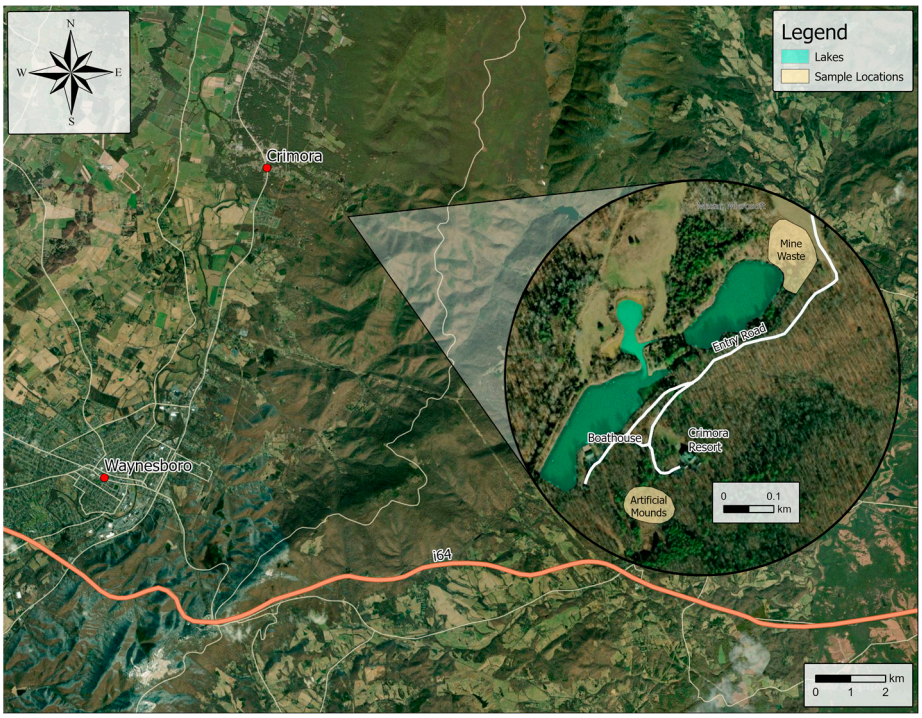


Figure 1. Map of selected sampling sites in the southern end of the Crimora ore deposit.



(**a**) (**b**)

Figure 2. (**a**) Mn nodules scattered in the southern bound of the Crimora ore deposit. (**b**) Sample is dark-black fine-to-medium-grained round and oblong nodules coated with a very fine-grained intermix of yellowish earthy limonite, clays, and quartz.

2.2. Geologic Setting

Crimora, VA, lies beneath Turk Mountain and the Shenandoah National Park. It is located on terrace deposits and alluvial fans. The terrace deposits (thickness 0–6 m) are dissected remnants of unconsolidated, stratified alluvial deposits of clays, silts, and sands with quartzite gravel at the base. Alluvial fans (0–60 m) are unconsolidated, locally dissected, poorly stratified overlapping deposits of clays, silt, and sand with interbedded quartzite cobbles and boulders [26].

Crimora deposit mainly consists of rounded "psilomelane" nodules mixed with quartz, clays, and limonite. The deposit lies into synclines overlaid by unconsolidated residual thick troughs of clays from the weathering of lower Cambrian dolomite, limestone, and shale in the Elbrook Formation. Quartzite in the Erwin Formation forms the bedrock [23].

The Crimora ore body is shown as irregular pockets, separate beds, and lenses within clay beds on quartzite cobbles and boulders in an elliptical basin located in a cone-shaped

syncline (Figure 3). The Mn-ores occur underneath the alluvial fans at the contact of the Cambrian-age Elbrook formation. The large concentration of the Crimora manganese (Mn) deposit may be related to the pair of transverse faults in the Turk Gap [26]. In Augusta County, much of the Elbrook Formation adjacent to the Pulaski and Staunton faults is a breccia of the "Max Meadows tectonic breccia type" [27]. The fault breccia along the Max Meadows overthrust consists of a lower autoclastic zone comprising angular blocks and fractured masses of Elbrook limestone, dolomite, and an intervening zone of crush conglomerate composed chiefly of rounded fragments of limestone, dolomite, and phyllite [28].

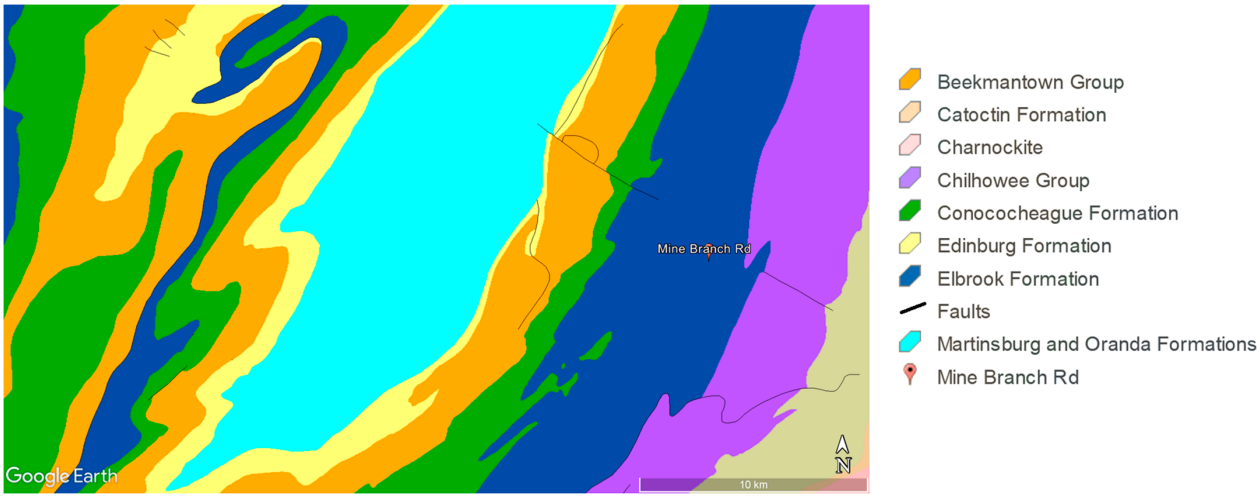


Figure 3. Geologic map of selected sampling site in the southern end of the Crimora ore deposit. The map is based on the U.S. Geological Survey (USGS) GIS database of geologic units, lithology, age, and structural features in Virginia [29].

2.3. X-ray Powder Diffraction (XRPD)

X-ray powder diffraction (XRPD) identified the samples' mineralogical composition. X-ray patterns were collected at room temperature using a Malvern PANalytical Empyrean diffractometer equipped with an X'Celerator detector and CuKα radiation (45 kV/40 mA) in facilities at the Department of Geology and Environmental Science, James Madison University. A Malvern PANAlytical Bragg-BrentanoHD incident beam optical module improved the peak-to-background ratio and the spectra intensity. Analyses of the samples were carried out with spinner-mode analysis, a 2θ scan range between 3° and 70°, a step size of 0.02° 2θ, a divergence slit of 0.5°, and incident beam anti-scatter slits of 2°. The fitted peak width for collected data was about 0.01° 2θ.

Quantitative mineralogical analyses were performed using PANalytical's HighScore Plus version 4.8 software [30]. Pure crystalline Al_2O_3 was chosen as an external standard and was analyzed under the same instrumental conditions as the sample. Figure 4 shows the mineralogy. The minerals' amount present in the Crimora sample is reported in Table 1.

Table 1. Mineralogical composition of Crimora sample. Standard deviation in parenthesis. All values have been rounded to the nearest unit.

Weight %	Sample
Quartz	34.3(4)
Goethite	17.8(6)
Illite	3.6(3)
Birnessite	1.3(5)
Hollandite	16.2(2)
Amorphous	26.7(3)

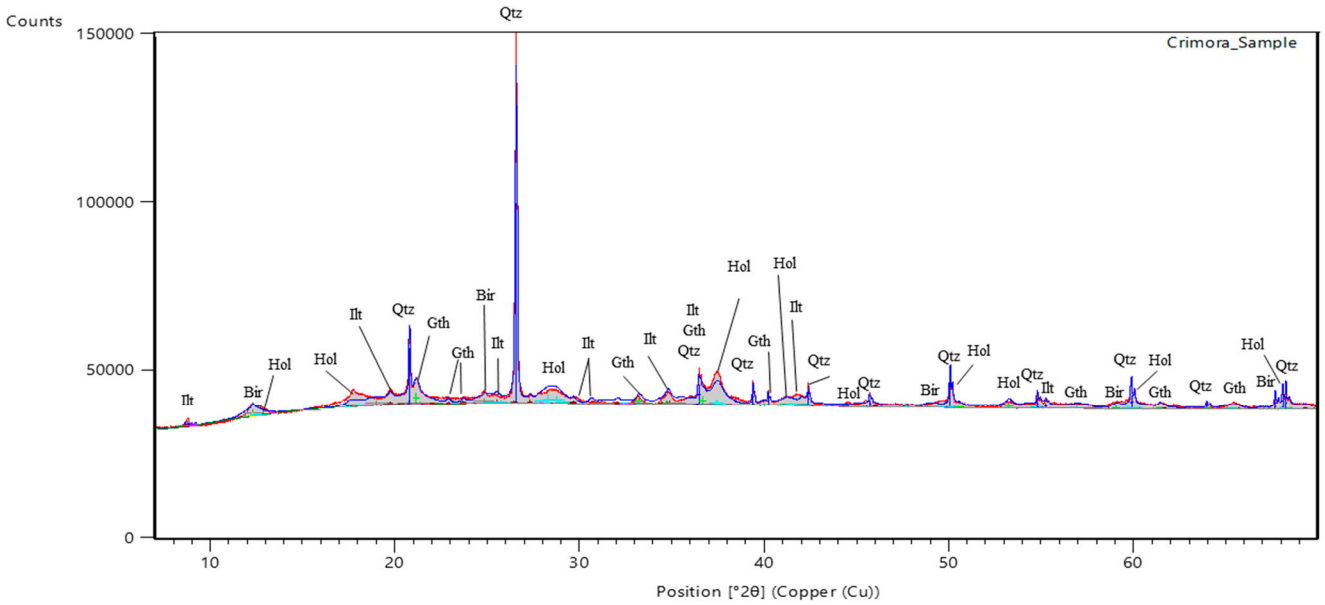


Figure 4. XRPD patterns for Crimora sample. Observed spectra (red line) and fitted spectra (blue solid line) are shown. Qtz = quartz; Ilt = illite; Bir = birnessite; Hol = hollandite; Gth = goethite.

2.4. Scanning Electron Microscopy (SEM)

An uncoated polished sample was mounted on carbon tape adhered to an aluminum stub and analyzed using a ZEISS Gemini SEM 360VP Scanning Electron Microscope (SEM) equipped with a field emission gun and Gemini 1 electron optical column. The instrument is located at the Department of Geology and Environmental Science, James Madison University, Harrisonburg, VA (USA). Backscattered electron (BSE) images were collected in a high vacuum at an accelerating voltage of 15 kV. The data were processed using the ZEISS SmartSEM version 7.00 software.

2.5. Inductively Coupled Plasma Optical Emission Spectroscopy (ICP-OES)

The Crimora ore sample was ground in an agate mortar and pestle to a fine powder before use. The sample (200 mg) was placed in Teflon reaction vessels, followed by 9.0 mL of HNO_3 (trace metal grade, Fisher Chemical Co., Pittsburgh, PA, USA) and 3.0 mL of HCl (trace metal grade, Fisher Chemical Co. Pittsburgh, PA, USA). The reaction vessels were sealed and heated in a CEM MARS-5 microwave-assisted digestion system. The temperature in the reaction vessels ramped for 5 min to 120 °C, where the temperature was held for 5 min. The temperature in the vessels was then increased to 175 °C with a 5-min 30-s ramp and held at 175 °C for 4 min and 30 s. After cooling, the contents of the vessels were transferred to 50 mL trace metal grade polypropylene centrifuge tubes and centrifuged for 20 min at 3000 RPM to remove suspended materials. Aliquots of the centrifuged solutions were placed into 10 mL trace metal grade centrifuge tubes for ICP-OES analysis. Then, 1:10 and 1:100 dilutions were made for each sample using 18 MΩ/cm^3 deionized water.

A Teledyne Leeman Labs Prodigy7 dual-view inductively coupled plasma optical emission spectrometer (ICP-OES) utilizing a high-energy Teledyne Leeman Labs Echelle Polychromator with an optical resolution of 0.007 nm @200 nm was used to obtain emission spectra from the digested Crimora ore sample. A peristaltic pump operating at 25 RPM introduced the samples through a glass cyclonic spray chamber before introduction to the concentric nebulizer and the torch. Power to the plasma was 1.2 kW, and the plasma gas flow was 14 L/min. Table 2 lists the wavelengths used, the viewing angle, and the detection limit for each reported metal.

Table 2. Analytical lines used for ICP-OES analysis.

Element	Wavelength (nm)	View	Detection Limit (mg/L)
Mn	257.610	Axial	0.00002
Fe	259.940	Axial	0.001
Ba	455.403	Radial	0.002
Ca	422.673	Radial	0.01
K	766.491	Radial	0.40
Na	589.592	Radial	0.07
Mg	279.553	Radial	0.0002
Y	371.030	Radial	0.004
Co	228.615	Axial	0.001
Ti	334.941	Axial	0.000028
Ni	231.604	Axial	0.002
Zn	206.200	Axial	0.0006
Cr	283.563	Axial	0.007
Li	670.784	Radial	0.002
W	207.911	Axial	0.001
Mo	202.030	Axial	0.0002
In	325.609	Axial	0.05
Tl	190.864	Axial	0.004
V	292.401	Axial	0.001
La	333.749	Axial	0.001
Ce	413.765	Radial	0.05

Single-element standards (1000 mg/L) were purchased from Inorganic Ventures, Christiansburg, VA, and used to prepare multielement stock solutions containing 100.0 mg/L of each metal and serially diluted when preparing standard curves. Ba, Ca, Mg, Na, K, Li, and Y were prepared in 2.5% HNO_3 containing 1000 mg/L Cs. Cs was added to control ionization interferences for elements with low ionization potentials. Co, Mn, Fe, and Zn were prepared in 2.5% HNO_3. Ti, Mo, Cr, and W were prepared in 2.5% HCl because these elements were stabilized as a chloride complex. San Joaquin Soil (NIST SRM 2709) was used as a control with each digest of eight samples. Percent recoveries were consistently between 90 and 105%. All chemicals and reagents were laboratory American Chemical Society (ACS) reagent grade. All glassware was washed with aqua regia and rinsed with deionized double distilled water before use.

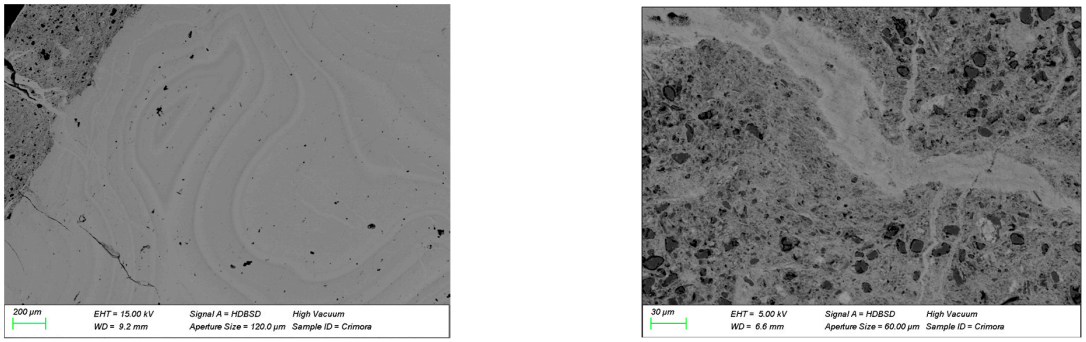
3. Results

3.1. Mn-Oxides Characterization

The genesis and mineralogy of manganese oxide deposits in the Shenandoah Valley is still uncertain. Thus, this study's clear mineralogical identification of the manganese oxides provided insights into the Mn minerals composing the Crimora deposit. The XRD pattern includes a low-intensity peak observed at 10° 2θ assigned to illite. High-intensity peaks of quartz and low-intensity peaks of goethite were present in all samples analyzed. The Mn-oxides identified are hollandite and birnessite (Figure 4). The minerals cryptomelane [$K(Mn^{4+}, Mn^{3+})_8O_{16}$], hollandite [$Ba(Mn^{4+}, Mn^{3+})_8O_{16}$], and coronadite [$Pb(Mn^{4+}, Mn^{3+})_8O_{16}$] are isostructural and form isomorphous mixtures [31]. Based on ICP-OES chemical analysis, we assigned the peaks at 12.72° 2θ, 17.7° 2θ, 28.7° 2θ, and 37.4° 2θ to hollandite.

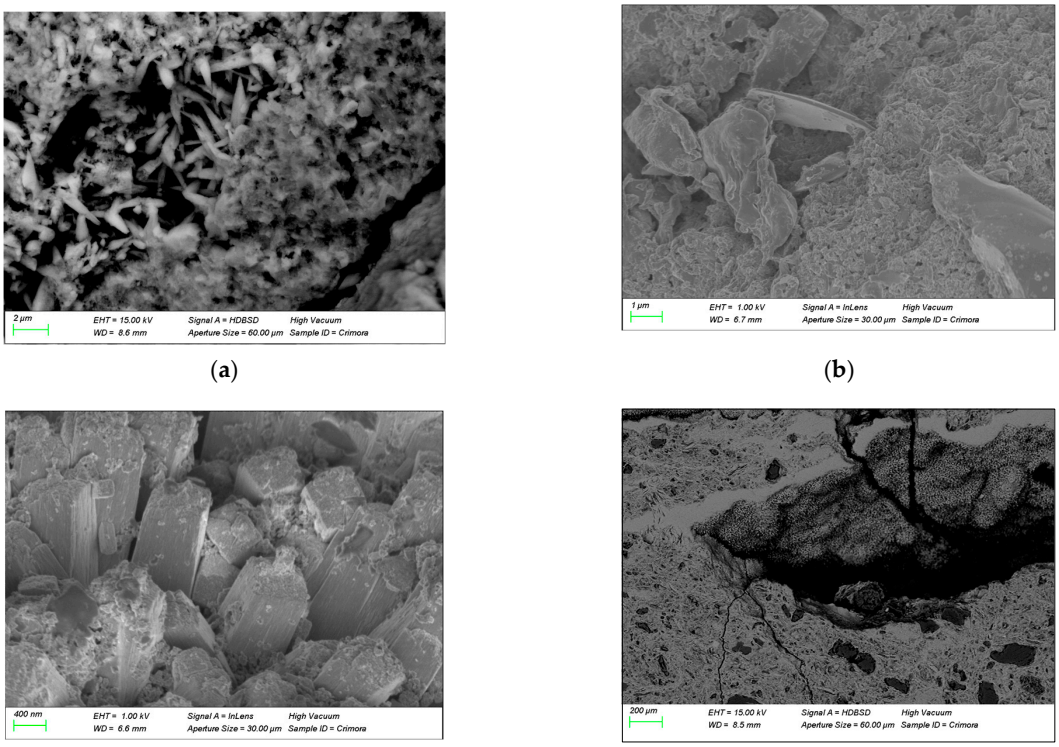
SEM investigations revealed that the Mn-oxides exhibit concentric layering also found in breccia matrices and veins (Figure 5). Aggregates of nano-sized radiating bladed and prismatic crystals of hollandite are found in cracks (Figure 6).

The genetic origin of the Mn deposit in Crimora, VA, was determined from the ICP-OES trace metal data. The ICP-OES data on Crimora manganese oxides are reported in Table 3. The average manganese concentration is 31.63 at%, and iron content is 4.73 at%. Data show Co, Zn, Cr, Li, Ti, Ni, V, In, Tl, La, and Y present as trace elements.



(**a**) (**b**)

Figure 5. Through SEM observations Crimora sample exhibits (**a**) banded layers. (**b**) Veins of hollandite (lighter gray) were found cutting the breccia matrix with scattered quartz crystals.



(**a**) (**b**)

(**c**) (**d**)

Figure 6. SEM images of Crimora sample showing (**a**) radiating nm-sized well-formed bladed crystals of hollandite; (**b**) a platy nm-sized crystal of birnessite; (**c**,**d**) square columnar nm-sized well-formed hollandite crystals found inside a crack.

Table 3. Chemical analyses of major, trace, and rare earth elements via ICP-OES.

Sample (n = 4)	at%	ppm
Mn	31.63	
Fe	4.73	
Ba	25.53	
Ca	0.22	
K	3.36	
Na	0.97	
Mg	0.17	
Ni		320.91
V		219.70
Co		1092.90

Table 3. *Cont.*

Sample (n = 4)	at%	ppm
Ti		789.64
Zn		891.95
Cr		116.33
Li		455.20
La		24.93
In		18,643.45
Tl		144.82
Y		374.92
Ce		bdl [1]
Mo		bdl [1]
W		bdl [1]

[1] bdl = below detection limit.

3.2. Formation Conditions

The irregular conglomerate Mn-oxides masses and lenses observed in the Crimora ore body suggest a complex origin with variable conditions. Genetic hypotheses for the Mn-mineralization can be established starting from paleogeographic and stratigraphic considerations. A bivariate analysis comparing chemical data from the literature and this study was carried out to shed light on the past environmental conditions under which the Crimora manganese oxides formed (Figure 7). Chemical data from the literature are compiled considering deep ocean (hydrothermal) samples [11,12,32–35], sedimentary supergene precipitated from freshwater [13,16,19,36,37], sedimentary supergene precipitated from seawater [16,37–40], and biogenic samples [41–44].

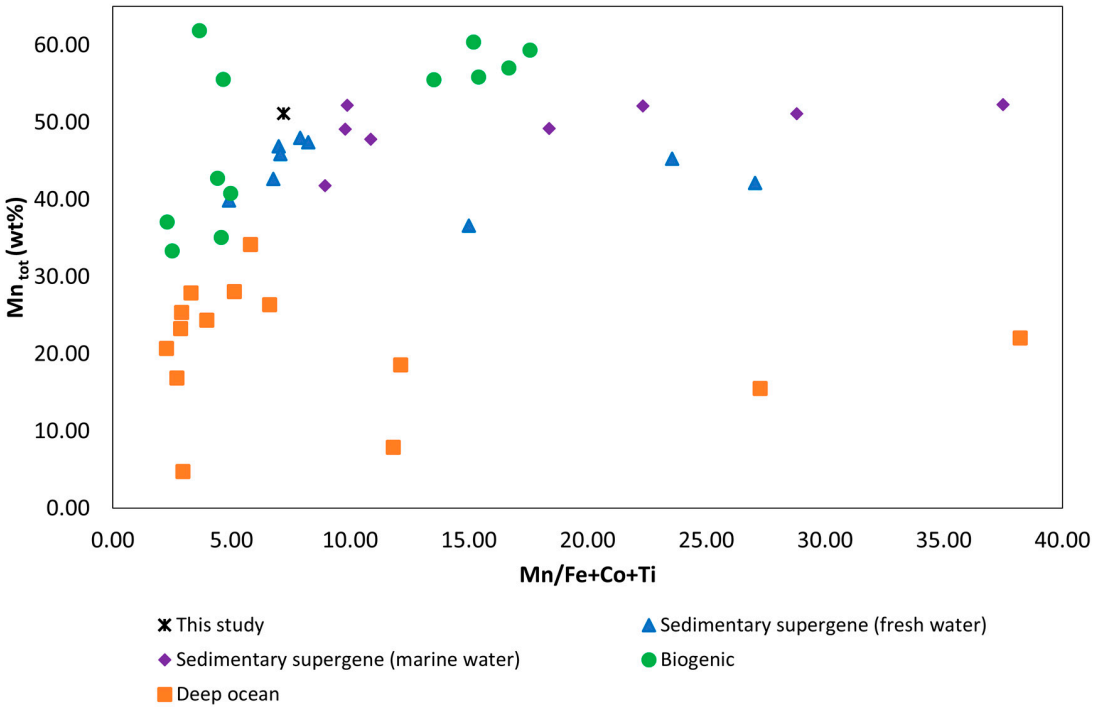


Figure 7. Bivariate plot of manganese abundance (wt%) vs. major substituting cations (i.e., Fe, Ti, Co) in manganese deposits with various genesis. Asterisk = this study; orange square = deep ocean (hydrothermal); blue triangle = sedimentary supergene (fresh water); purple diamond = sedimentary supergene (marine water); green circle = biogenic precipitation. Data from this study and deep ocean (hydrothermal) samples [11,12,32–35], sedimentary supergene precipitated from freshwater [13,16,19,36,37]; sedimentary supergene precipitated from seawater [16,37–40], and biogenic samples [41–44].

4. Discussion

Manganese mineralogy and geochemical features shed light on the specific genetic environment where Mn-oxides can form. Mn oxide/hydroxide are commonly referred to as Mn oxide minerals. They are found in various geological settings and occur as fine-grained aggregates, veins, marine and freshwater nodules and concretions, crusts, dendrites, and coatings on rock surfaces (e.g., desert varnish).

Mn oxide deposits occur in various geological settings. Sedimentary manganese deposits refer to those formed through precipitation in ambient pressure–temperature condition from water solutions enriched in dissolved manganese [5]. The most extensive deposition of Mn oxides today occurs in the oceans as nodules, micro concretions, coatings, and crusts [1]. Manganese nodules in deep-sea sediments exhibit a continuous mixing from diagenetic end-members, which contain the mineral todorokite and are enriched in Mn, Ni, and Cu, to hydrogenous end-members, which contain the mineral δ-MnO_2 (vernadite) and are enriched in Fe and Co. Mn oxide phases in ocean nodule form by catalytic oxidation and adsorption of Mn^{2+} on suitable substrates, such as mineral and rock fragments and fine-grained MnO_2 and $Fe(OH)_3$ [1]. The nodules are most abundant in oxygenated environments with low sedimentation rates and reach their greatest concentration in deep-water at or below the calcium carbonate compensation depth (4000–6000 m) [45]. The Mn source in ocean nodules is likely continental runoff and hydrothermal and volcanic activity at midocean spreading centers [1].

Dark brown to black fine-grained mixtures (mainly birnessite, hollandite, romanèchite, and todorokite) formed under oxidizing conditions have been reported covering cave walls, stream clasts, and other speleothems in caves [46]. Furthermore, some bacterial species in the cave environment can catalyze the oxidation and precipitation of Fe and Mn nodules. The aqueous solution's pH and/or redox conditions control this biologically mediated process [46].

Mohamed and Paleologos [47] observed that common minerals in soils are birnessite, lithiophorite, hollandite, todorkite, and pyrolusite. The hollandite supergroup includes several Mn^{4+} and Ti oxides, often referred to as tunnel oxides due to their structural features [48]. According to Biagioni et al. [48], the name hollandite should be applied to the member of the coronadite group having Ba as the dominant tunnel cation. Hollandite minerals can be major phases in the oxidized zones of Mn deposits and important ores [1]. Birnessite-like minerals are common phyllomanganates in surficial soils and sediments that mediate important environmental processes (e.g., biogeochemical cycles and heavy metal confinement). Ca is the dominant interlayer cation in both biotic and abiotic birnessites, especially when they precipitate in the presence of shallow-water carbonate-rich sediments [49]. Birnessite and hollandite occur in both acid and alkaline soils, whereas lithiophorite seems to be favored by neutral-to-acidic conditions. Lithiophorite appears to take up Co and Cu more effectively than hollandite within an acidic pH range (pH 4–6) [50]. Birnessite-like oxides in soils and sediments exhibit large surface areas and participate in several oxidation-reduction and cation-exchange reactions. The cation exchange capacity of phyllomanganates is enhanced at alkaline pH (i.e., pH 8.3, similar to that of seawater) and exceeds that of swelling clays [1,49].

Supergene settings include weathering and deposition in subaerial, marine, lacustrine, and palustrine conditions. Supergene deposits develop at the expense of primary ores when these are uplifted and become exposed to the action of meteoric agents [51]. The availability of meteoric fluids controls the alteration of the primary deposit, followed by the precipitation of secondary mineral phases in the form of carbonates, oxides, and silicates [17]. In modern marine sediments, Mn is an oxyhydroxide in slowly accumulating (pelagic) sediments of the deep ocean and in surficial deposits of continental margin environments. Diagenetic recycling of Mn causes surficial deposits to have higher Mn enrichments than in many pelagic sediments [52]. The diagenetic deposits partially derive their metals from the recycling through the interstitial sediment waters and water initially contained in organic matter that is decaying and dissolving in the sediments, whereas the

hydrogenous deposits uptake metals from seawater or diagenetically unenriched interstitial waters. Bacteria can also contribute to the diagenetic behavior of Mn in sedimentary deposits [53].

XRPD patterns of Crimora samples show hollandite and birnessite as the main Mn-oxide phases (Figure 4). Paragenetic minerals such as quartz, illite, and goethite are associated with the Mn-oxides. Quantitative analysis performed via the Rietveld method shows that the main minerals in Crimora samples are hollandite (16.2 wt%) and birnessite (1.3 wt%), as well as goethite (17.8 wt%) and quartz (34.3 wt%). Hollandite is generally associated with goethite and is typically found within sedimentary deposits [47]. Birnessite is frequently observed in terrestrial manganese deposits, weathering zones, and soils [1,54,55]. Given the minerals' assemblage of Crimora samples observed via XRPD, the genesis of these minerals is consistent with supergene marine–terrestrial oxidation zone conditions. Several Mn-oxides in surface environments are poorly crystalline and of biogenic origin [56,57]. The amorphous phase (26.7 wt%) and the low-intensity broad peaks associated with the Mn-oxides indicate that the Mn-oxides analyzed are poorly crystalline, and their nucleation may be controlled by biogenic activity in a sedimentary setting.

Scanning electron microscopy (SEM) examination of a polished sample revealed that Mn-oxides in Crimora exhibit banded layers (Figure 5a). Veins of hollandite (lighter gray) were found cutting the breccia matrix with scattered quartz crystals (Figure 5b). Radiating nm-sized well-formed bladed crystals of hollandite (Figure 6a), a platy nm-sized crystal of birnessite (Figure 6b), as well as square columnar nm-sized well-formed hollandite crystals (Figure 6c) were found inside a crack (Figure 6d). No evidence of biological morphologies (e.g., dendritic layers, filaments, micropores, and micro dome-shaped stromatolite-like structure) was observed, indicating primarily inorganic precipitation of the Mn-oxides.

Freshwater, seawater, and hydrothermal fluids have distinctive and contrasting geochemical signatures. The concentration and range of dissolved chemical species available for the reaction determine which cations are adsorbed by the manganese oxides. Manganese oxide minerals with a MnO_x-like formula have a high adsorbing capacity for trace metals such as Ni, Co, Ti, Fe, and Zn [20–24]. In this manner, the adsorbed chemical species impart a geochemical signature to the Mn-oxides, representing the depositional fluid composition [4,19,39,58,59]. The concentration of Mn and other substituting cations (e.g., Fe, Co, Ti, Ni) is different for Mn-oxides precipitated from freshwater, seawater, or hydrothermal fluid, and therefore, provides a diagnostic tool to shed light on the genetic origin of Mn-oxides [19,36,39,58,59]. Figure 7 shows a mixed origin of the Crimora sample in different environments with varying biological and sedimentary supergene (freshwater and marine) conditions. A limited difference was shown in the concentration of Mn and other metals in samples forming in freshwater or marine water sedimentary environments (Figure 7). Data suggest that the Mn-rich deposits in Crimora, VA, were formed in a brine mineral system in an ancient sedimentary basin intensely modified by structural deformation through the Max Meadows overthrust and recrystallized in mixed seawater and freshwater supergene conditions. This complex origin with variable genetic conditions agrees with the surrounding geologic setting where the irregular conglomerate masses and lenses are concentrated in the Crimora ore body.

Ferromanganese oxides of different genetic origins are characterized by distinctive compositions of trace elements [7,39]. Several factors, such as the rate of precipitation, the nature of geochemical components in oxides (e.g., Mn-oxides, Fe-oxyhydroxides, and detrital minerals), speciation of elements in seawater and hydrothermal fluid, are mainly responsible for such compositional variation. Nicholson [58] observed that hydrothermal manganese oxide deposits characteristically show geochemical enrichments in the assemblage As-Ba-Cu-Li-Mo-Pb-Sb-Sr-V-Zn and a Mn-As geochemical association. Supergene marine deposits show Na-K-Ca-Mg-Sr and Co-Cu-Ni geochemical enrichments. Supergene terrestrial deposits tend to have very high Ba contents and an Mn-Ba association. Manganese oxides derived from the weathering of dubhites (a base and precious ore minerals and gangue) contain high levels of Pb and Zn. Mn-As diagnostic correlation was observed

for hydrothermal deposits [58]. Diagenetic processes cause the enrichment of Mn, Ti, and Ni in manganese deposits, whereas an enrichment of trace elements could be related to adsorption from pore water [40,58]. Samsaz et al. [39] and Samsaz et al. [19] observed a positive correlation of Mn-Ba-Sr-Co-Cu-Ni in the Nikopol deposit (Ukraine) and Chiatura deposit (Georgia), which is similar to diagenetic Mn deposits formed in shallow marine environments. In Crimora samples, a Ba concentration of 25.53 at%, as well as significant amounts of Fe, Mg, Ca, K, and Na, were shown via ICP-OES analysis (Table 3). According to Nicholson [58], Samsaz et al. [39], and Samsaz et al. [19], the average geochemical composition of Crimora Mn-oxides is consistent with a supergene marine–terrestrial fluid source.

Manganese minerals in sedimentary environments may contain variable major, trace, and rare earth element (REE) concentrations owing to the Mn substitutions [39]. Y and Ce could be used as geochemical indicators of a sedimentary environment, tectonic evolution, percolation of hydrothermal fluids, and freshwater in ferromanganese deposits [60]. High concentrations of Y (average 201 ppm) and Ce (average 1204 ppm) were observed in association with Mn, Fe, Cu, Co, and Ni in nodules collected in the Northwestern Pacific [61]. These authors observed that the geochemical assemblage significantly correlates with authigenic seawater precipitation origin in ferromanganese deposits. Sasmaz et al. [19] observed that redox potential can affect Y and Ce concentrations. In briny waters, Ce is oxidized to Ce^{4+}, whose solubility is low, and thus, it results in a Ce depletion in the deposit. According to Sasmaz et al. [19], Ce depletion is a strong indicator of an oxic depositional environment, typical to near seawater/freshwater-sediment interface, whereas Ce enrichment indicates anoxic conditions specific to the hydrothermal or deep ocean environment. A Ce depletion was observed by Gültekin and Balcı [40] in Binkılıç, Trache Basin, Turkey, and it was attributed to terrigenous sediments transported in a mixed depositional oxic/anoxic environment. Sjöberg et al. [62] observed the precipitation for microbially mediated birnessite-type Mn oxide enriched in yttrium (Y) in a tunnel to the main shaft of the former Ytterby mine in Sweden. A high concentration of yttrium (Y = 374.92 ppm) was observed in the Crimora sample, whereas Ce was not detected, supporting the supergene continental marine–terrestrial genesis of the sample under study. The observed enrichment of Y in the Crimora samples can be ascribed to a possible microbially mediated precipitation of hollandite from supergene marine–terrestrial fluids in the primary ore body.

ICP-OES data also show substantial enrichments of Co, Li, Ba, Cr, V, and Ni (Table 3), which is consistent with the diagnostic geochemical plots in Figure 7, indicating a mixed sedimentary supergene and biogenic genesis of Crimora manganese oxides. The high concentration of K and Na corroborates the prominent supergene sedimentary marine–terrestrial origin of the Crimora ore deposit.

5. Conclusions

This paper is the first detailed study of Crimora manganese deposits conducted since the mine was closed in the 1950s. Modern geochemical and mineralogical methods, XRPD, SEM, ICP-OES, and bivariate analysis, have been used to elucidate the genesis of the Mn oxides in the Crimora ore body. XRPD patterns show that the main Mn-oxides in the samples are hollandite (16.2 wt%) and birnessite (1.3%). The XRPD data further show the presence of an amorphous phase (26.7 wt%), quartz (34.3%), goethite (17.8%), and illite (3.6%). The high amorphous content and broad low-intensity peaks assigned to hollandite and birnessite are ascribed to the typical poor crystallinity of Mn-oxides.

The distinctive Mn and trace metal compositions of freshwater, seawater, and hydrothermal fluids shed light on Mn-oxides' genetic origin. Hydrothermal manganese oxide deposits generally show geochemical enrichments in the assemblage As-Ba-Cu-Li-Mo-Pb-Sb-Sr-V-Zn and an Mn-As geochemical correlation. Supergene marine deposits show Na-K-Ca-Mg-Sr and Co-Cu-Ni geochemical enrichments. In contrast, supergene terrestrial deposits tend to have very high Ba contents and an Mn-Ba geochemical affinity. Y and Ce enrichments are associated with Mn, Fe, Cu, Co, and Ni geochemical assemblage in

ferromanganese deposits with authigenic seawater precipitation origin. The ICP-OES data of Crimora samples show concentrations of trace elements such as Co, Ba, Zn, Cr, Li, La, In, V, Tl, and Y. Ba concentration is 25.53 at%, confirming the presence of hollandite. A high yttrium concentration (Y = 375 ppm) was observed in Crimora samples, whereas Ce was not detected, supporting the mixed supergene continental marine–terrestrial genesis of the sample under study. The significant amounts of Fe, Ca, K, Na, and Mg shown via ICP-OES analysis corroborate the prominent supergene sedimentary marine–terrestrial origin of the Crimora ore deposit. Bivariate analysis, based on the geochemical correlation of Mn and other common substituting cations (e.g., Fe, Co, Ti) in samples with a strictly hydrothermal, sedimentary, and biogenic origin, revealed that Crimora manganese oxides have an affinity with Mn-oxides with sedimentary supergene and biogenic genesis. The Crimora sample shows the best agreement with the literature values for samples precipitated in freshwater or marine sedimentary environments.

Data from this study suggest that the Mn-rich deposit in Crimora, VA, was formed in an ancient sedimentary basin brine mineral system intensely modified by structural deformation through the Max Meadows overthrust and recrystallized in mixed biogenic and supergene conditions. The surrounding geologic setting of alluvial fans composed of irregular conglomerate masses and lenses of limestone and dolomite, concentrated above the Crimora Mn-rich ore body, agrees with this complex origin with various genetic conditions. Future investigations will examine the age when Crimora Mn-oxides formed.

Author Contributions: Conceptualization, C.E. and R.D.F.J.; methodology, C.E. and R.D.F.J.; validation, C.E. and R.D.F.J.; investigation, C.E., J.R.W., M.T.M. and R.D.F.J.; data curation, C.E. and R.D.F.J.; writing—original draft preparation, C.E. and J.R.W.; writing—review and editing, C.E. and R.D.F.J.; visualization, C.E., J.R.W., M.T.M. and R.D.F.J.; supervision, C.E. and R.D.F.J. All authors have read and agreed to the published version of this manuscript.

Funding: This research received no external funding.

Data Availability Statement: Not applicable.

Acknowledgments: This research was carried out at James Madison University. Crimora Mine Retreat is kindly acknowledged for providing access to the surrounding woodland that was previously part of the southern bound of open-pit manganese mines. Anonymous reviewers are kindly acknowledged for their comments and suggestions.

Conflicts of Interest: The authors declare no conflict of interest.

References

1. Post, J.E. Manganese Oxide Minerals: Crystal Structures and Economic and Environmental Significance. *Proc. Natl. Acad. Sci. USA* **1999**, *96*, 3447–3454. [CrossRef] [PubMed]
2. Sun, W.; Kitchaev, D.A.; Kramer, D.; Ceder, G. Non-Equilibrium Crystallization Pathways of Manganese Oxides in Aqueous Solution. *Nat. Commun.* **2019**, *10*, 573. [CrossRef]
3. Lu, A.; Li, Y.; Liu, F.; Liu, Y.; Ye, H.; Zhuang, Z.; Li, Y.; Ding, H.; Wang, C. The Photogeochemical Cycle of Mn Oxides on the Earth's Surface. *Mineral. Mag.* **2021**, *85*, 22–38. [CrossRef]
4. Roy, S. Genetic Diversity of Manganese Deposition in the Terrestrial Geological Record. *Geol. Soc. Lond. Spec. Publ.* **1997**, *119*, 5. [CrossRef]
5. Roy, S. Sedimentary Manganese Metallogenesis in Response to the Evolution of the Earth System. *Earth-Sci. Rev.* **2006**, *77*, 273–305. [CrossRef]
6. Ghosh, S.K. Diversity in the Family of Manganese Oxides at the Nanoscale: From Fundamentals to Applications. *ACS Omega* **2020**, *5*, 25493–25504. [CrossRef] [PubMed]
7. Bau, M.; Schmidt, K.; Koschinsky, A.; Hein, J.; Kuhn, T.; Usui, A. Discriminating between Different Genetic Types of Marine Ferro-Manganese Crusts and Nodules Based on Rare Earth Elements and Yttrium. *Chem. Geol.* **2014**, *381*, 1–9. [CrossRef]
8. Roy, S. Environments and Processes of Manganese Deposition. *Econ. Geol.* **1992**, *87*, 1218–1236. [CrossRef]
9. Cannon, W.F.; Kimball, B.E.; Corathers, L.A. *Manganese—Critical Mineral Resources of the United States—Economic and Environmental Geology and Prospects for Future Supply*; Professional Paper; U.S. Department of the Interior U.S. Geological Survey: Reston, VA, USA, 2017; pp. L1–L28.
10. Roy, S. Manganese Metallogenesis: A Review. *Ore Geol. Rev.* **1988**, *4*, 155–170. [CrossRef]

11. Hein, J.R.; Koschinsky, A.; Kuhn, T. Deep-Ocean Polymetallic Nodules as a Resource for Critical Materials. *Nat. Rev. Earth Environ.* **2020**, *1*, 158–169. [CrossRef]
12. Hein, J.R.; Spinardi, F.; Okamoto, N.; Mizell, K.; Thorburn, D.; Tawake, A. Critical Metals in Manganese Nodules from the Cook Islands EEZ, Abundances and Distributions. *Ore Geol. Rev.* **2015**, *68*, 97–116. [CrossRef]
13. Xu, H.; Peng, X.; Ta, K.; Song, T.; Du, M.; Li, J.; Chen, S.; Qu, Z. Structure and Composition of Micro-Manganese Nodules in Deep-Sea Carbonate from the Zhaoshu Plateau, North of the South China Sea. *Minerals* **2020**, *10*, 1016. [CrossRef]
14. Halbach, P.E.; Jahn, A.; Cherkashov, G. Marine Co-Rich Ferromanganese Crust Deposits: Description and Formation, Occurrences and Distribution, Estimated World-Wide Resources. In *Deep-Sea Mining: Resource Potential, Technical and Environmental Considerations*; Sharma, R., Ed.; Springer International Publishing: Cham, Switzerland, 2017; pp. 65–141, ISBN 978-3-319-52557-0.
15. Crerar, D.A.; Barnes, H.L. Deposition of Deep-Sea Manganese Nodules. *Geochim. Cosmochim. Acta* **1974**, *38*, 279–300. [CrossRef]
16. Pracejus, B. Nature and Formation of Supergene Manganese Deposits on Groote Eylandt. Ph.D. Thesis, University of Adelaide, Adelaide, Australia, 1989.
17. De Putter, T.; Ruffet, G.; Yans, J.; Mees, F. The Age of Supergene Manganese Deposits in Katanga and Its Implications for the Neogene Evolution of the African Great Lakes Region. *Ore Geol. Rev.* **2015**, *71*, 350–362. [CrossRef]
18. Pharoe, B.K.; Evdokimov, A.N.; Gembitskaya, I.M.; Bushuyev, Y.Y. Mineralogy, Geochemistry and Genesis of the Post-Gondwana Supergene Manganese Deposit of the Carletonville-Ventersdorp Area, North West Province, South Africa. *Ore Geol. Rev.* **2020**, *120*, 103372. [CrossRef]
19. Sasmaz, A.; Sasmaz, B.; Hein, J.R. Geochemical Approach to the Genesis of the Oligocene-Stratiform Manganese-Oxide Deposit, Chiatura (Georgia). *Ore Geol. Rev.* **2021**, *128*, 103910. [CrossRef]
20. Harder, E.C. *Manganese Deposits of the United States, with Sections on Foreign Deposits, Chemistry, and Uses*; Bulletin; US Government Printing Office: Washington, DC, USA, 1910; pp. 58–61.
21. Hack, J.T. Geomorphology of the Shenandoah Valley Virginia and West Virginia and Origin of the Residual Ore Deposits. *US Geol. Surv. Prof. Pap.* **1965**, *484*, 89.
22. Hewett, D.F. *Some Manganese Miners in Virginia and Maryland*; Bulletin; U.S. Department of the Interior: Burlington, MA, USA; U.S. Geological Survey: Menlo Park, CA, USA, 1916; pp. 37–71.
23. Stose, G.W.; Miser, H.D.; Katz, F.J.; Hewe'Tt, D.F. *Manganese Deposits of the West Foot of the Blue Ridge, Virginia*; Bulletin; Virginia Geological Survey: Charlottesville, VA, USA, 1919; p. 206.
24. USGS National Minerals Information Center Manganese Statistics and Information. Available online: https://www.usgs.gov/centers/national-minerals-information-center/manganese-statistics-and-information (accessed on 10 May 2023).
25. Judd, E.K. Engineering and Mining Journal. *McGraw-Hill Publ. Co.* **1907**, *83*, 478–479.
26. Gathright II, T.M.; Henika, W.S.; Sullivan, J.L., III. Publication 013: Geology of the Crimora Quadrangle, Virginia 1978. Available online: https://www.energy.virginia.gov/commercedocs/PUB_13.pdf (accessed on 28 March 2023).
27. Virginia Division of Mineral Resources Geologic Map of Virginia: Virginia Division of Mineral Resources 1993. Available online: https://mrdata.usgs.gov/geology/state/geog-units.html (accessed on 28 March 2023).
28. Cooper, B.N.; Haff, J.C. Max Meadows Fault Breccia. *J. Geol.* **1940**, *48*, 945–974. [CrossRef]
29. U.S. Geological Survey (USGS) Virginia Geologic Map Data. Available online: https://mrdata.usgs.gov/geology/state/state.php?state=VA (accessed on 26 July 2023).
30. Degen, T.; Sadki, M.; Bron, E.; König, U.; Nénert, G. The HighScore Suite. *Powder Diffr.* **2014**, *29*, S13–S18. [CrossRef]
31. Gruner, J.W. The Chemical Relationship of Cryptomelane (Psilomelane), Hollandite, and Coronadite. *Am. Mineral.* **1943**, *28*, 497–506.
32. Bonatti, E.; Zerbi, M.; Kay, R.; Rydell, H. Metalliferous Deposits from the Apennine Ophiolites: Mesozoic Equivalents of Modern Deposits from Oceanic Spreading Centers. *Geol. Soc. Am. Bull.* **1976**, *87*, 83. [CrossRef]
33. Monget, J.-M.; Murray, J.W.; Mascle, J. *A World-Wide Compilation of Published, Multicomponent/Analyses of Ferromanganese Concrétions*; NSF-IDOE Manganese Nodule Project: Scripps Institution of Oceanography: La Jolla, CA, USA, 1976.
34. Piper, D.Z.; Leong, K.; Cannon, W.F. Manganese Nodule and Surface Sediment Compositions: Domes sites A, B, and C. In *Marine Geology and Oceanography of the Pacific Manganese Nodule Province*; Marine Science; Bischoff, J.L., Ed.; Plenum Publishing Corporation: New York, NY, USA, 1979; pp. 437–474. Available online: https://store.pangaea.de/Projects/NOAA-MMS/chp_10.1007_978-1-4684-3518-4_13.pdf (accessed on 24 January 2023).
35. Cronan, D.S. Sedimentary Rocks | Oceanic Manganese Deposits. In *Encyclopedia of Geology*; Selley, R.C., Cocks, L.R.M., Plimer, I.R., Eds.; Elsevier: Oxford, UK, 2005; pp. 113–120, ISBN 978-0-12-369396-9.
36. Nicholson, K. An Ancient Manganese-Iron Deposit of Freshwater Origin, Islay, Argyllshire. *Scott. J. Geol.* **1988**, *24*, 175. [CrossRef]
37. Ostwald, J. Manganese Oxide Mineralogy, Petrography and Genesis, Pilbara Manganese Group, Western Australia. *Miner. Deposita* **1993**, *28*, 198–209. [CrossRef]
38. Marescotti, P.; Frezzotti, M.L. Alteration of Braunite Ores from Eastern Liguria (Italy) during Syntectonic Veining Processes: Mineralogy and Fluid Inclusions. *Eur. J. Mineral.* **2000**, *12*, 341–356. [CrossRef]
39. Sasmaz, A.; Zagnitko, V.M.; Sasmaz, B. Major, Trace and Rare Earth Element (REE) Geochemistry of the Oligocene Stratiform Manganese Oxide-Hydroxide Deposits in the Nikopol, Ukraine. *Ore Geol. Rev.* **2020**, *126*, 103772. [CrossRef]
40. Gultekin, A.H.; Balcı, N. Geochemical Characteristics of Sedimentary Manganese Deposit of Binkılıç, Trache Basin, Turkey. *J. Geol. Geophys.* **2018**, *7*, 1000336. [CrossRef]

41. Gázquez, F.; Calaforra, J.M.; Forti, P. Black Mn-Fe Crusts as Markers of Abrupt Palaeoenvironmental Changes in El Soplao Cave (Cantabria, Spain). *Int. J. Speleol.* **2011**, *40*, 163–169. [CrossRef]
42. Ivarsson, M.; Broman, C.; Gustafsson, H.; Holm, N.G. Biogenic Mn-Oxides in Subseafloor Basalts. *PLoS ONE* **2015**, *10*, e0128863. [CrossRef]
43. Biondi, J.C.; Polgári, M.; Gyollai, I.; Fintor, K.; Kovács, I.; Fekete, J.; Mojzsis, S.J. Biogenesis of the Neoproterozoic Kremydilite Manganese Ores from Urucum (Brazil)—A New Manganese Ore Type. *Precambrian Res.* **2020**, *340*, 105624. [CrossRef]
44. Scholtysik, G.; Dellwig, O.; Roeser, P.; Arz, H.W.; Casper, P.; Herzog, C.; Goldhammer, T.; Hupfer, M. Geochemical Focusing and Sequestration of Manganese during Eutrophication of Lake Stechlin (NE Germany). *Biogeochemistry* **2020**, *151*, 313–334. [CrossRef]
45. Cronan, D.S. Manganese Nodules☆. In *Encyclopedia of Ocean Sciences*, 3rd ed.; Cochran, J.K., Bokuniewicz, H.J., Yager, P.L., Eds.; Academic Press: Oxford, UK, 2019; pp. 607–614, ISBN 978-0-12-813082-7.
46. Onac, B.P. Chapter 84—Minerals in Caves. In *Encyclopedia of Caves (Third Edition)*; White, W.B., Culver, D.C., Pipan, T., Eds.; Academic Press: Cambridge, MA, USA, 2019; pp. 699–709, ISBN 978-0-12-814124-3.
47. Mohamed, A.-M.O.; Paleologos, E.K. Chapter 4—The Soil System. In *Fundamentals of Geoenvironmental Engineering*; Mohamed, A.-M.O., Paleologos, E.K., Eds.; Butterworth-Heinemann: Oxford, UK, 2018; pp. 89–127, ISBN 978-0-12-804830-6.
48. Biagioni, C.; Capalbo, C.; Pasero, M. Nomenclature Tunings in the Hollandite Supergroup. *Eur. J. Mineral.* **2013**, *25*, 85–90. [CrossRef]
49. Elmi, C.; Post, J.E.; Heaney, P.J.; Ilton, E.S. Effects of PH and Ca Exchange on the Structure and Redox State of Synthetic Na-Birnessite. *Am. Mineral.* **2021**, *106*, 15–27. [CrossRef]
50. Lidiard, H.M.; Rae, J.E.; Parker, A. Identification of Mn-Oxide Minerals in Some Soils from Devon, UK, and Their Varying Capacity to Adsorb Co and Cu. *Enviro. Geochem. Health* **1993**, *15*, 93–104. [CrossRef] [PubMed]
51. Lelong, F.; Tardy, Y.; Grandin, G.; Trescases, J.J.; Boulange, B. Pedogenesis, Chemical Weathering and Processes of Formation of Some Supergene Ore Deposits. In *Supergene and Surficial Ore Deposits*; Elsevier: Amsterdam, The Netherlands, 1976; pp. 93–173, ISBN 978-0-444-41403-8.
52. Calvert, S.E.; Pedersen, T.F. Sedimentary Geochemistry of Manganese; Implications for the Environment of Formation of Manganiferous Black Shales. *Econ. Geol.* **1996**, *91*, 36–47. [CrossRef]
53. Crerar, A.D.; Cormick, K.R.; Barnes, L.H. Organic controls on the sedimentary geochemistry of manganese. *Acta Mineral.-Petrogr.* **1972**, *20*, 217–226.
54. Ostwald, J. Some Observations on the Chemical Composition of Todorokite. *Mineral. Mag.* **1986**, *50*, 336–340. [CrossRef]
55. Scheinost, A.C.; Singh, B. Metal Oxides. In *Reference Module in Earth Systems and Environmental Sciences*; Elsevier: Amsterdam, The Netherlands, 2022; ISBN 978-0-12-409548-9.
56. Tebo, B.M.; Bargar, J.R.; Clement, B.G.; Dick, G.J.; Murray, K.J.; Parker, D.; Verity, R.; Webb, S.M. BIOGENIC MANGANESE OXIDES: Properties and Mechanisms of Formation. *Annu. Rev. Earth Planet. Sci.* **2004**, *32*, 287–328. [CrossRef]
57. Shiller, A.M.; Stephens, T.H. Microbial Manganese Oxidation in the Lower Mississippi River: Methods and Evidence. *Geomicrobiol. J.* **2005**, *22*, 117–125. [CrossRef]
58. Nicholson, K. Contrasting Mineralogical-Geochemical Signatures of Manganese Oxides; Guides to Metallogenesis. *Econ. Geol.* **1992**, *87*, 1253–1264. [CrossRef]
59. Gultekin, A.H. Mineralogical and Chemical Doses Are Used to Determine the Origins of Manganese Deposits. *Geol. Eng.* **1998**, *50*, 39–46.
60. Zhong, Y.; Chen, Z.; Gonzalez, F.J.; Zheng, X.; Li, G.; Luo, Y.; Mo, A.; Xu, A.; Wang, S. Rare Earth Elements and Yttrium in Ferromanganese Deposits from the South China Sea: Distribution, Composition and Resource Considerations. *Acta Oceanol. Sin.* **2018**, *37*, 41–54. [CrossRef]
61. Ren, J.; He, G.; Deng, X.; Deng, X.; Yang, Y.; Yao, H.; Yang, S. Metallogenesis of Co-Rich Ferromanganese Nodules in the Northwestern Pacific: Selective Enrichment of Metallic Elements from Seawater. *Ore Geol. Rev.* **2022**, *143*, 104778. [CrossRef]
62. Sjöberg, S.; Callac, N.; Allard, B.; Smittenberg, R.H.; Dupraz, C. Microbial Communities Inhabiting a Rare Earth Element Enriched Birnessite-Type Manganese Deposit in the Ytterby Mine, Sweden. *Geomicrobiol. J.* **2018**, *35*, 657–674. [CrossRef]

Disclaimer/Publisher's Note: The statements, opinions and data contained in all publications are solely those of the individual author(s) and contributor(s) and not of MDPI and/or the editor(s). MDPI and/or the editor(s) disclaim responsibility for any injury to people or property resulting from any ideas, methods, instructions or products referred to in the content.